DALTON
FULL PAPER

Cleavage of homometallic and formation of heterometallic M–M bonds. Serendipitous syntheses of bimetallic $MnPd(\mu\text{-}PPh_2)(CO)_4(\eta^2\text{-}P\text{–}P)$ (P–P = dppm, dppe, dppf) and polymetallic $Mn_2Pd_2Ag(\mu\text{-}Cl)(\mu\text{-}PPh_2)_2(\mu\text{-}dppm)(CO)_8$

Ye Liu, Kim Hun Lee, Jagadese J. Vittal and Tzi Sum Andy Hor *

Department of Chemistry, National University of Singapore, Kent Ridge, 119260, Singapore. E-mail: andyhor@nus.edu.sg

Received 26th February 2002, Accepted 22nd April 2002
First published as an Advance Article on the web 20th May 2002

Condensation of $[Mn_2(CO)_8(\mu\text{-}PPh_2)]^-$ with Pd(II) assisted by Ag(I) leads to cluster disproportionation, *viz.* $Mn_2Pd_2Ag(\mu\text{-}Cl)(\mu\text{-}PPh_2)_2(\mu\text{-}dppm)(CO)_8$ and $MnPd(\mu\text{-}PPh_2)(CO)_4(\eta^2\text{-}P\text{–}P)$ (P–P = dppm, dppe, dppf). The former shows a distorted bow-tie structure with two heterometallic triangles {AgPdMn} sharing an Ag center. The unexpected phosphide migration across different metals holds the key to the cleavage and formation of metal–metal bonds. The bimetallic complexes are stabilized by all common diphosphines whereas the polymetallic structure is isolated only when supported by dppm. The latter shows three different types of heterometal–metal bonds Ag–Mn (2.6938(4) Å), Ag–Pd (2.7637(1) Å) and Mn–Pd (2.8183(9) Å) (average values).

Introduction

Emerging significance in metallic nanomaterials[1] and bimetallic catalysis[2] continues to shape the development of intermetallic chemistry[3] and fuel our interest in hetero(poly)metallic complexes.[4] We recently reported a redox-condensation-type mechanism whereby some unusual multimetallic networks can be built based on a dinuclear precursor $[Mn_2(CO)_8(\mu\text{-}PPh_2)]^-$ and Au(I).[5] We subsequently extended this approach to related Pd(II), but encountered an unexpectedly different outcome. Instead of preserving the electron-rich $[Mn_2(\mu\text{-}PPh_2)]$ moiety, which is widely perceived to be stable and robust, we observed a redox process that precludes the formation of the expected $[PdMn_2(PPh_2)]$ or $[Pd_2Mn_2(PPh_2)]$ entities. During the process, we also observed a serendipitous polynuclear product that incorporates the third metal, *viz.* Ag(I), which was intended as a substrate. These results illustrate the complications in heteropolymetallic syntheses based on seemingly obvious redox condensation. Even with stable supporting bridging ligands such as phosphide,[6] fragmentation of M–M bonds can occur. When fragmentation is accompanied by re-assembly, and if homometallic M–M bond rupture is replaced by heterometallic M–M bond formation, we can envisage the formation of thermodynamically driven heteromultimetallic architectures.

Results and discussion

Chloride abstraction reactions of $PdCl_2(\eta^2\text{-}P\text{–}P)$ [P–P = Ph_2PXPPh_2, X = CH_2 (dppm), C_2H_4 (dppe), $Fe(C_5H_4)_2$ (dppf)] with $AgNO_3$ (1 : 2) followed by condensation with $[Mn_2(CO)_8(PPh_2)]^-$ at room temperature (Scheme 1) give bimetallic complexes $MnPd(\mu\text{-}PPh_2)(CO)_4(\eta^2\text{-}P\text{–}P)$ in 4 (**1a**), 11 (**1b**) and 10% (**1c**) yields respectively. In the case of P–P = dppm, an unexpected cluster $Mn_2Pd_2Ag(\mu\text{-}Cl)(\mu\text{-}PPh_2)_2(\mu\text{-}dppm)(CO)_8$ (**2a**) was also isolated in 15% yield. No other major products were identified although some unknown minor byproducts are present. Complexes **1a**–**1c** are new but their PR_2H (R = Ph, Cy) derivatives were reported previously by Braunstein *et al.*,[7] who used a different route *via* oxidation of pre-formed Pd–Mn bonds with PR_2H.

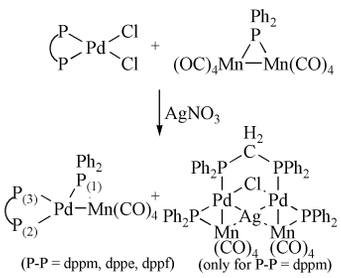

Scheme 1 Condensation of $PdCl_2(\mu\text{-}P\text{–}P)$ with $PPN^+[Mn_2(CO)_8(\mu\text{-}PPh_2)]^-$.

The ^{31}P NMR spectra of **1a**, **1b** and **1c** (Fig. 1) invariably show three discrete resonances, *viz.* a downfield doublet for the bridging phosphide (P_{Ph}), and two doublets of doublets for the diphosphine P_{trans} and P_{cis} with respect to the Pd–Mn bond. The magnitude of the *J*(PP) coupling constants is in agreement with a transoid P(2)–Pd–μ-P(1) arrangement. X-Ray single-crystal crystallographic analyses of **1b** (Fig. 2) and **1c** (Fig. 3) pointed to a common structure: a Mn–Pd bonded bimetallic complex supported by bridging phosphide, chelating phosphine on Pd and terminal carbonyls on Mn. The higher bite demand of the dppf ligand in **1c** forces the chelating angle (P(2)–Pd–P(3)) to open up from 86.74(2)° in **1b** to 102.81(4)° in **1c** and lengthen, presumably weakening, the Mn–Pd bond from 2.6589(4) to 2.7672(7) Å, see Table 1. It is notable that despite the different steric demands for all three diphosphines, they invariably opt to take up the chelating mode instead of the obvious alternative of forming a bridge over the Mn–Pd bond. Although the structures of the PR_2H derivatives were not established crystallographically, that of the isoelectronic $MoPd(\mu\text{-}PCy_2)(\eta\text{-}Cp)(CO)_2(PCy_2H)_2$ has been reported to give a much longer Mo–Pd bond (2.916(2) Å).[8] The strength of the $[MnPd(\mu\text{-}PPh_2)]$ entity could help to explain the formation of **1**. Although an obvious intermediate is the direct condensation

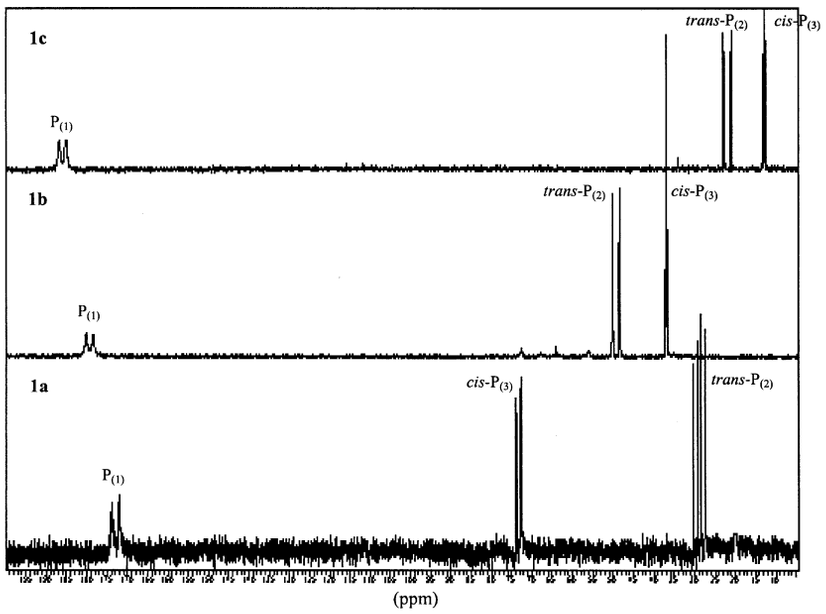

Fig. 1 ^{31}P NMR spectra of bimetallic $MnPd(\mu\text{-}PPh_2)(CO)_4(\eta^2\text{-}P\text{–}P)$ (P–P = dppm (**1a**), dppe (**1b**), dppf (**1c**)).

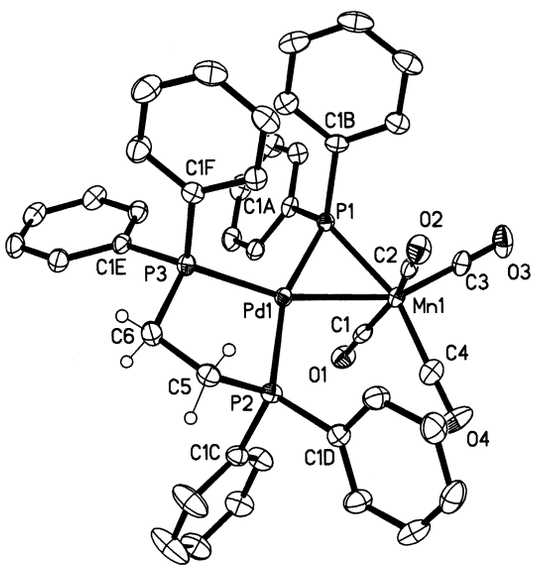

Fig. 2 Molecular structure of $MnPd(\mu\text{-}PPh_2)(CO)_4(\eta^2\text{-dppe})$ (**1b**) (ellipsoids at the 50% probability level).

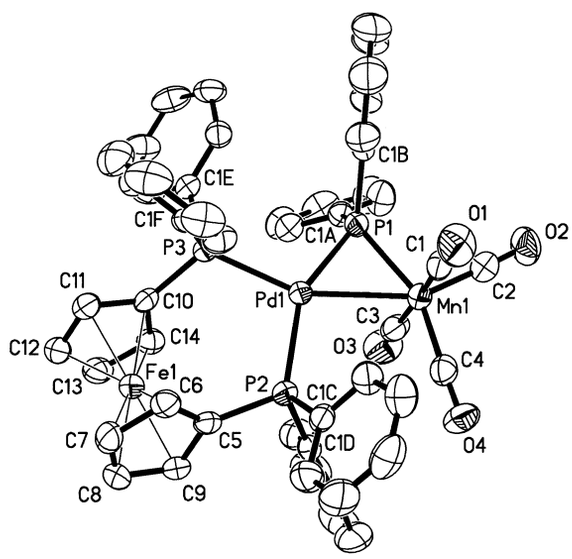

Fig. 3 Molecular structure of $MnPd(\mu\text{-}PPh_2)(CO)_4(\eta^2\text{-dppf})\cdot(CH_3)_2CO$ (**1c**·$(CH_3)_2CO$) (ellipsoids at the 50% probability level).

product *viz.* $[(\eta^2\text{-P–P})Pd(\mu\text{-}PPh_2)Mn_2(CO)_n]^+$, there is no observable evidence for its formation. Presumably a rapid migratory process of the phosphide from Mn to Pd paves the way for a facile departure of a stable $Mn(CO)_m^+$, giving rise to **1**.

Complexes **1** are generally stable as solids but slowly decompose in solution. The stability decreases in the order **1b** > **1c** ⩾ **1a**, suggesting that a four-membered ring with an acute chelating angle is unfavorable. This is consistent with the observation and isolation of **2a**, which is supported by a bridging dppm ligand. The equivalent dppe or dppf analogues could not be isolated. The ^{31}P NMR spectrum of **2a** gives a unique spectrum with two resonances corresponding to the bridging phosphide [P_{Ph} (s)] and two equivalent phosphorus nuclei on dppm [$P_{Pd\text{–}Pd}$ (d)]. X-Ray crystallographic analysis revealed an unusual and unexpected pentanuclear trimetallic cluster of $Mn_2Pd_2Ag(\mu\text{-Cl})(\mu\text{-}PPh_2)_2(\mu\text{-dppm})(CO)_8$ (**2a**, Fig. 4), It comprises a distorted bow-tie structure with two heterometallic triangles {AgPdMn} (dihedral angle $\theta = 11.3°$) sharing a common Ag center. Similar to **1**, there are terminal carbonyls on Mn and bridging phosphides supporting the Mn–Pd bonds. However,

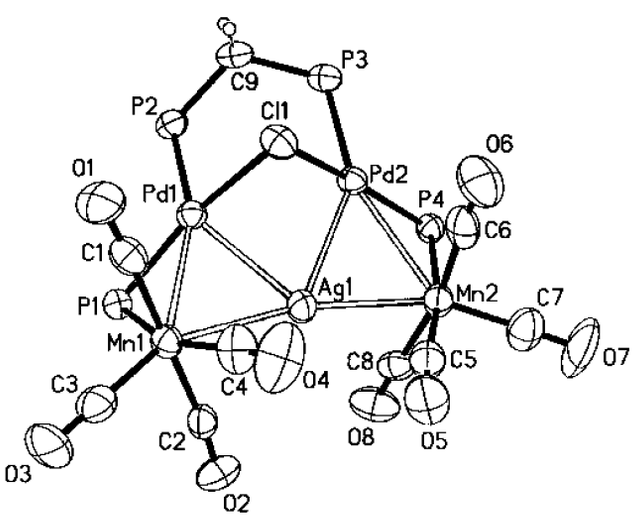

Fig. 4 Molecular structure of $Mn_2Pd_2Ag(\mu\text{-Cl})(\mu\text{-}PPh_2)_2(\mu\text{-dppm})(CO)_8\cdot(CH_3)_2CO$ (**2a**·$(CH_3)_2CO$) (ellipsoids at the 50% probability level).

Table 1 Selected bond lengths (Å) and bond angles (°) for **1b**, **1c** and **2a**

$MnPd(\mu\text{-}PPh_2)(CO)_4(\eta^2\text{-dppe})$, **1b**					
Mn(1)–Pd(1)	2.6589(4)	Pd(1)–P(1)	2.2820(6)	Pd(1)–P(2)	2.3121(6)
Mn(1)–P(1)	2.2465(7)	Pd(1)–P(3)	2.2945(6)	Mn(1)–C (average)	1.818
Mn(1)–Pd(1)–P(1)	53.428(17)	Mn(1)–Pd(1)–P(2)	107.706(18)	Pd(1)–Mn(1)–C(1)	89.21(7)
Pd(1)–Mn(1)–P(1)	54.667(17)	Mn(1)–Pd(1)–P(3)	163.204(19)	Pd(1)–Mn(1)–C(2)	73.45(7)
Mn(1)–P(1)–Pd(1)	71.91(2)	P(2)–Pd(1)–P(1)	161.13(2)	Pd(1)–Mn(1)–C(3)	155.61(8)
P(2)–Pd(1)–P(3)	86.74(2)	P(3)–Pd(1)–P(1)	111.81(2)	Pd(1)–Mn(1)–C(4)	104.43(8)
$MnPd(\mu\text{-}PPh_2)(CO)_4(\eta^2\text{-dppf})$, **1c**					
Mn(1)–Pd(1)	2.7672(7)	Pd(1)–P(1)	2.2654(11)	Pd(1)–P(3)	2.3388(10)
Mn(1)–P(1)	2.2216(12)	Pd(1)–P(2)	2.3641(11)	Mn(1)–C (average)	1.801
Mn(1)–Pd(1)–P(1)	51.21(3)	Mn(1)–Pd(1)–P(2)	100.64(3)	Pd(1)–Mn(1)–C(1)	92.10(13)
Pd(1)–Mn(1)–P(1)	52.64(3)	Mn(1)–Pd(1)–P(3)	156.47(3)	Pd(1)–Mn(1)–C(2)	154.37(14)
Mn(1)–P(1)–Pd(1)	76.15(4)	P(2)–Pd(1)–P(1)	151.50(4)	Pd(1)–Mn(1)–C(3)	86.61(13)
P(2)–Pd(1)–P(3)	102.81(4)	P(3)–Pd(1)–P(1)	105.53(4)	Pd(1)–Mn(1)–C(4)	103.83(14)
$Mn_2Pd_2Ag(\mu\text{-}Cl)(\mu\text{-}PPh_2)_2(\mu\text{-dppm})(CO)_8$, **2a**					
Pd(1)–Mn(1)	2.7934(9)	Pd(1)–Cl(1)	2.4695(15)	Pd(1)–P(2)	2.3416(15)
Pd(2)–Mn(2)	2.8432(9)	Pd(2)–Cl(1)	2.4760(15)	Pd(2)–P(3)	2.3140(15)
Ag(1)–Mn(1)	2.7246(9)	Mn(1)–P(1)	2.2426(18)	Mn(1)–C(average)	1.819
Ag(1)–Mn(2)	2.6629(9)	Mn(2)–P(4)	2.2430(17)	Mn(2)–C(average)	1.824
Ag(1)–Pd(1)	2.7259(6)	Pd(1)–P(1)	2.2295(16)		
Ag(1)–Pd(2)	2.8014(6)	Pd(2)–P(4)	2.2057(16)		
Pd(1)–Ag(1)–Mn(1)	61.66(2)	Pd(1)–Mn(1)–P(1)	51.14(4)	Mn(1)–Ag(1)–Pd(2)	130.97(3)
Pd(2)–Ag(1)–Mn(2)	62.65(2)	Pd(2)–Mn(2)–P(4)	49.70(4)	Mn(2)–Ag(1)–Pd(1)	133.06(3)
Mn(1)–Pd(1)–Ag(1)	59.15(2)	Mn(1)–Pd(1)–P(1)	51.56(4)	Ag(1)–Pd(1)–P(1)	92.49(4)
Mn(2)–Pd(2)–Ag(1)	56.29(2)	Mn(2)–Pd(2)–P(4)	50.85(4)	Ag(1)–Pd(2)–P(4)	97.71(4)
Pd(1)–Mn(1)–Ag(1)	59.19(2)	Ag(1)–Pd(1)–Cl(1)	73.67(4)	Ag(1)–Mn(1)–P(1)	92.23(5)
Pd(2)–Mn(2)–Ag(1)	61.06(2)	Ag(1)–Pd(2)–Cl(1)	72.22(4)	Ag(1)–Mn(2)–P(4)	100.85(5)
Pd(1)–P(1)–Mn(1)	77.31(6)	Pd(1)–Cl(1)–Pd(2)	80.58(5)	Mn(1)–Pd(1)–P(2)	160.46(5)
Pd(2)–P(4)–Mn(2)	79.45(6)	Ag(1)–Pd(1)–P(2)	138.03(4)	Mn(2)–Pd(2)–P(3)	156.37(5)
Mn(1)–Ag(1)–Mn(2)	164.62(3)	Ag(1)–Pd(2)–P(3)	146.42(4)	Mn(1)–Pd(1)–Cl(1)	102.49(4)
Pd(1)–Ag(1)–Pd(2)	70.688(16)			Mn(2)–Pd(2)–Cl(1)	111.63(4)

the dppm ligand has taken up a more natural position [8] in bridging over a non-bonding Pd ··· Pd axis (3.1981(6) Å). As a result, the two heterometallic triangles are connected by dppm and chloride. The supporting role of dppm cannot be replaced by the other ligands we have attempted, which is indicative of the uniqueness of a short diphosphine like dppm. In this 74-electron cluster, the six M–M bonds are distributed evenly among the three types of heterometallic bonds (Ag–Pd, Ag–Mn and Mn–Pd). These would account for 18-electron Pd and Mn as well as 14-electron Ag. The lengthening and presumably weakening of the Mn–Pd bonds (2.7934(9) Å and 2.8432(9) Å), compared to **1b** (2.6589(4) Å) and **1c** (2.7672(7) Å) are consistent with a delocalized structure similar to that of the $\{AuMn_4\}$ cluster we described earlier.[9] The short Ag–Pd bond lengths (2.7259(6) and 2.8014(6) Å) compared to the reported Ag(I)–Pd(II) bonds (*ca.* 2.8 to 3.1 Å),[10] when supplemented by typical Ag–Mn bonds (2.7246(9) and 2.6629(9) Å),[11] collectively result in a compact intermetallic network locked by bridging phosphide and dppm ligands. It also provides a thermodynamic explanation for the migratory process of phosphide from Mn to Pd.

Although the formation of **2a** can be treated as a concerted attack of two units of **1a** across the Ag–Cl bond of AgCl, followed by phosphine dissociation and migration as well as formation of metal–metal bonds, we have no firm evidence of this mechanistic conjecture. All attempts to prepare **2a** from **1a** and AgCl have so far failed. The possibility that **2a** could arise from facile attack of the planar dinuclear $[(\eta^2\text{-P–P})_2Pd_2(\mu\text{-Cl})_2]^{2+}$, which behaves like unsaturated Pd upon cleavage of the Pd–Cl bridges,[12] by the anionic Mn_2 precursor in the presence of adventitious Ag^+ is being explored. This alternative is supported by indirect evidence when we could not obtain **2a** under conditions that promote complete chloride abstraction (*e.g.* with excess $AgNO_3$).

Experimental

General procedures and materials

All reactions were performed under pure nitrogen using standard Schlenk techniques. $Mn_2(CO)_8(\mu\text{-H})(\mu\text{-}PPh_2)$ [13] and $PPN^+[Mn_2(CO)_8(\mu\text{-}PPh_2)]^-$ [14] were prepared by literature methods. $PdCl_2(\eta^2\text{-P–P})$ (P–P = dppm, dppe, dppf) were prepared from $PdCl_2(CH_3CN)_2$ and the diphosphine. All other reagents were commercial products and were used as received. Some of the microanalytical data of the chemically pure samples were not completely satisfactory, despite repeated analyses. One possible reason is the interference from the different metallic elements present.

FT-IR and NMR spectroscopy

FT-IR spectra were recorded on a Perkin-Elmer 1600 spectrometer using KBr plates. All NMR spectra were recorded in $CDCl_3$ solution on a Bruker ACF 300 MHz spectrometer. The ^{31}P NMR chemical shifts were externally referenced to 85% H_3PO_4. Elemental analyses were performed by the analytical service of this department. Pre-coated silica TLC plates of layer thickness 0.25 mm were obtained from Merck or Baker.

X-Ray crystallography

The diffraction experiments for the samples **1b**, **1c** and **2a** were carried out on a Bruker AXS CCD diffractometer with Mo-Kα ($\lambda = 0.71073$Å) radiation. The program SMART [15] was used for the collection of data frames, indexing reflections and the determination of lattice parameters, SAINT [15] for the integration of intensity of reflection and scaling, SADABS [16] for absorption correction and SHELXTL [17] for space group and structure determination and refinements. Crystal data and refinement details are given in Table 2.

Table 2 Data collection and structure refinement of $MnPd(\mu\text{-}PPh_2)(CO)_4(\eta^2\text{-dppe})$ (**1b**), $MnPd(\mu\text{-}PPh_2)(CO)_4(\eta^2\text{-dppf})$ (**1c**) and $Mn_2Pd_2Ag(\mu\text{-}Cl)(\mu\text{-}PPh_2)_2(\mu\text{-dppm})(CO)_8$ (**2a**)

	1b	**1c**·$(CH_3)_2CO$	**2a**·$(CH_3)_2CO$
Chemical formula	$C_{42}H_{34}MnO_4P_3Pd$	$C_{53}H_{44}FeMnO_5P_3Pd$	$C_{60}H_{48}AgClMn_2O_9P_4Pd_2$
Formula weight	856.94	1070.98	1502.86
Crystal system	Triclinic	Monoclinic	Monoclinic
Space group	$P\bar{1}$	$P2_1/c$	$P2_1/c$
T/K	223(2)	223(2)	223(2)
a/Å	10.0096(5)	13.4500(6)	11.3130(4)
b/Å	10.2022(5)	10.7239(5)	26.5117(10)
c/Å	18.7467(10)	33.3018(15)	19.9718(7)
α/°	92.351(1)	90	90
β/°	95.620(1)	92.5950(10)	91.478(1)
γ/°	94.809(1)	90	90
V/Å^3	1896.16(17)	4798.4(4)	5988.1(4)
Z	2	4	4
ρ/g cm^{-3}	1.501	1.482	1.667
μ/mm^{-1}	0.975	1.075	1.526
No. of reflections collected	18173	27407	34997
No. of unique data R(int)	6660 (0.0258)	8445 (0.0472)	10548 (0.0789)
$R1/wR2$ (obs. data)	0.0265, 0.0706	0.0420, 0.0580	0.0524, 0.0770
(all data)	0.0295, 0.0714	0.0636, 0.0604	0.0846, 0.0843

CCDC reference numbers 180412–180414.

See http://www.rsc.org/suppdata/dt/b2/b202001g/ for crystallographic data in CIF or other electronic format.

Syntheses

$MnPd(\mu\text{-}PPh_2)(CO)_4(\eta^2\text{-dppm})$ (1a) and $Mn_2Pd_2Ag(\mu\text{-}Cl)(\mu\text{-}PPh_2)_2(\mu\text{-dppm})(CO)_8$ (2a). To a pale yellow solution of $PdCl_2(\eta^2\text{-dppm})$ (0.169 g, 0.3 mmol) in CH_3CN (30 ml), $AgNO_3$ (0.102 g, 0.6 mmol) was added. The mixture was stirred for *ca*. 1 h before filtering dropwise into a flask containing a yellow solution of $PPN[Mn_2(CO)_8(\mu\text{-}PPh_2)]$ (PPN = $N(PPh_3)_2$) (0.317 g, 0.3 mmol) in CH_3CN (30 ml). The resultant dark-red mixture was further stirred at room temperature for 1 h and then stripped of solvent to give a reddish brown residue, which was dissolved in a minimum amount of acetone and separated on silica TLC plates with acetone/hexane (3 : 7) eluant. The major yellow and orange bands were extracted with acetone to give **1a** (yield: 4%) and **2a** (yield: 15%). The crystals of **2a**·$(CH_3)_2CO$ were obtained from acetone/hexane.

Anal. Calcd for **1a**: C, 58.42; H, 3.83. Found: C, 57.38; H, 3.81%. ^{31}P NMR (δ): 27.3, 28.5, 29.2, 30.3 (dd, P_2, *trans* $^2J_{PP}$ = 220 Hz, $^2J_{PP}$ = 139 Hz); 72.6, 72.8, 73.8, 74.0 (dd, P_3, *cis* $^2J_{PP}$ = 27 Hz, $^2J_{PP}$ = 137 Hz); 172.1, 174.0 (d, P_1, br, *trans* $^2J_{PP}$ = 228 Hz). IR (CO, cm^{-1}): 1962 s, 1884 vs, 1870 s (solid KBr). Anal. Calcd for **2a**·$(CH_3)_2CO$: C, 47.95; H, 3.22. Found: C, 47.91; H, 3.21%. ^{31}P NMR (δ): 27.9, 28.3 (d, $^2J_{PP}$ = 53 Hz, P_{Pd-Pd}); 218.0 (s, br, P_{Ph}). IR (CO, cm^{-1}): 2021 vs, 2006 s, 1930 vs, 1913 vs (solid KBr).

$MnPd(\mu\text{-}PPh_2)(CO)_4(\eta^2\text{-dppe})$ (1b). $AgNO_3$ (0.102 g, 0.6 mmol) was added to a solution of $PdCl_2(\eta^2\text{-dppe})$ (0.173 g, 0.3 mmol) in CH_3CN (30 mL). After stirring for 1 h, the clear yellow solution was transferred into $PPN[Mn_2(CO)_8(\mu\text{-}PPh_2)]$ (0.317 g, 0.3 mmol) in CH_3CN (30 mL). The mixture was stirred at 60 °C for 24 h. After filtration the resultant reddish brown solution was evaporated *in vacuo* to give a residue which was redissolved in a minimum amount of acetone, coated onto TLC plates and eluted with acetone/hexane (3 : 7). The separated major orange band was extracted and recrystallized from acetone/hexane to give orange crystals. Yield: 11%.

Anal. Calcd for **1b**: C, 58.86; H, 4.00. Found: C, 58.68; H, 4.01%. ^{31}P NMR (δ): 36.6, 36.8, 37.0 (dd, P_3, *cis* $^2J_{PP}$ = 27 Hz, $^2J_{PP}$ = 23 Hz); 48.3, 48.5, 50.0, 50.2 (dd, P_2, *trans* $^2J_{PP}$ = 210 Hz, $^2J_{PP}$ = 23 Hz); 178.5, 180.2 (d, P_1, br, *trans* $^2J_{PP}$ = 214 Hz). IR (CO, cm^{-1}): 1998 s, 1926 vs, 1895 vs.

$MnPd(\mu\text{-}PPh_2)(CO)_4(\eta^2\text{-dppf})$ (1c). $AgNO_3$ (0.102 g, 0.6 mmol) was added to a solution of $PdCl_2(\eta^2\text{-dppf})$ (0.110 g, 0.3 mmol) in CH_3CN (30 mL). After stirring for 1 h, the clear yellow solution was transferred into a CH_3CN (30 mL) solution of $PPN[Mn_2(CO)_8(\mu\text{-}PPh_2)]$ (0.317 g, 0.3 mmol). The mixture was stirred at 60 °C for 24 h, filtered, and stripped of solvent under vacuum. The residue was coated onto TLC plates and eluted with acetone/hexane (3 : 7). The major orange band was extracted and crystallized from acetone/hexane to give orange crystals. Yield: 10%.

Anal. Calcd for **1c**: C, 59.29 H, 3.78. Found: C, 58.29; H, 3.78%. ^{31}P NMR (δ): 12.4, 12.7, 13.0 (dd, P_3, *cis* $^2J_{PP}$ = 34 Hz, $^2J_{PP}$ = 38 Hz); 20.9, 21.2, 22.6, 22.9 (dd, P_2, *trans* $^2J_{PP}$ = 208 Hz, $^2J_{PP}$ = 38 Hz); 185.1, 186.9 (d, P_1, br, *trans* $^2J_{PP}$ = 202 Hz). IR (CO, cm^{-1}): 2011 s, 1920 vs, 1902 vs.

Acknowledgements

The authors acknowledge the National University of Singapore (NUS) for financial support. Technical support from the Department of Chemistry of NUS is appreciated.

References

1 K. E. Drexler (Editor), *Nanosystems, Molecular Machinery, Manufacturing, and Computation*, Wiley, New York, 1992; G. Schmid (Editor), *Clusters and Colloids: from theory to applications*, VCH, Weinheim, New York, 1994; P. Braunstein, L. A. Oro and P. R. Raithby (Editors), *Metal Clusters in Chemistry Vol. 3 – Nanomaterials and solid-state cluster chemistry*, Wiley-VCH, Weinheim, New York, 1999.

2 J. P. Fackler, Jr. (Editor), *Metal-Metal Bonds and Clusters in Chemistry and Catalysis*, Plenum Press, New York, 1990; A. Fukuoku, T. Sadashima, T. Sugiura, X. Xu, Y. Mizuho and S. Komiya, *J. Organomet. Chem.*, 1994, **473**, 139; P. Braunstein, L. A. Oro and P. R. Raithby (Editors), *Metal Clusters in Chemistry Vol. 2 – Catalysis and dynamics and physical properties of metal clusters*, Wiley-VCH, Weinheim, New York, 1999; R. D. Adams and F. A. Cotton (Editors), *Catalysis by Di- and Polynuclear Metal Cluster Complexes*, Wiley-VCH, New York, 1998.

3 N. Wheatley and P. Kalck, *Chem. Rev.*, 1999, **99**, 3379; H. Nakano, A. Nakamura and K. Mashima, *Inorg. Chem.*, 1996, **35**, 4007; M. Sommovigo, M. Pasquali, F. Marchetti, P. Leoni and T. Beringhelli, *Inorg. Chem.*, 1994, **33**, 2651; J. Powell, J. F. Sawyer and S. J. Smith, *J. Chem. Soc., Dalton Trans.*, 1992, 2793.

4 Z. Li, Z. H. Loh, K. F. Mok and T. S. A. Hor, *Inorg Chem.*, 2000, **39**, 5299; Z. Li, X. Xu, S. B. Khoo, K. F. Mok and T. S. A. Hor, *J. Chem. Soc., Dalton Trans*, 2000, 2901; S. W. A. Fong, W. T. Yap, J. J. Vittal, T. S. A. Hor, W. Henderson, A. G. Oliver and C. E. F. Rickard, *J. Chem. Soc., Dalton Trans*, 2001, 1986; J. Zhang, Y. H. Zhang, X. N. Chen, E. R. Ding and Y. Q. Yin, *Organometallics*, 2000, **19**, 5032.

5 K. H. Lee, P. M. N. Low and T. S. A. Hor, *Organometallics*, 2001, **20**, 3250.

6 P. Braunstein, E. de Jésus, A. Dedieu, M. Lanfranchi and A. Tiripicchio, *Inorg. Chem.*, 1992, **31**, 399; T. Blum, P. Braunstein, A. Tiripicchio and M. T. Camellini, *Organometallics*, 1989, **8**, 2504.
7 P Braunstein, E. de Jésus, A. Tiripicchio and M. T. Camellini, *J. Organomet. Chem.*, 1989, **368**, C5.
8 P. Braunstein, C. M. Bellefon, B. Oswald and M. Ries, *Inorg. Chem.*, 1993, **32**, 1638.
9 P. M. N. Low, A. L. Tan, T. S. A. Hor, Y. S. Wen and L. K. Liu, *Organometallics*, 1996, **15**, 2595.
10 M. Ebihara, K. Tokoro, M. Maeda, M. Ogami, K. Imaeda, K. Sakurai, H. Masuda, T. Kawamura and M. Glaum, *J. Chem. Soc., Dalton Trans.*, 1994, 3621; M. Ebihara, M. Tsuchiya, M. Yamada, K. Tokoro and T. Kawamura, *Inorg. Chim. Acta*, 1995, **231**, 35; J. E. Kickham and S. J. Loeb, *Organometallics*, 1995, **14**, 3584; W. Kläui, B. W. Skelton and A. H. White, *Aust. J. Chem.*, 1997, **50**, 1047.
11 U. Florke and D. Petters, *Acta Crystallogr., Sect. C*, 2001, **57**, 1044.
12 G. Wilkinson, F. G. A. Stone and E. W. Abel (Editors), in *Comprehensive Organometallic Chemistry: the synthesis, reactions, and structures of organometallic compounds*, Pergamon, New York, 1st edn., 1982, vol. 6, 240.
13 J. A. Iggo, M. J. Mays, P. R. Raithby and K. J. Hendrick, *J. Chem. Soc., Dalton Trans.*, 1983, 205.
14 J. A. Iggo, M. J. Mays, P. R. Raithby and K. J. Hendrick, *J. Chem. Soc., Dalton Trans.*, 1984, 633.
15 SMART & SAINT Software Reference Manuals, Version 4.0, Siemens Energy & Automation, Inc., Analytical Instrumentation, Madison, WI, 1996.
16 G. M. Sheldrick,; SADABS, software for empirical absorption correction, University of Göttingen, Göttingen, Germany, 1996.
17 SHELXTL Reference Manual, Version 5.03, Siemens Energy & Automation, Inc., Analytical Instrumentation, Madison, WI, 1996.